







UDC 528.8.042.1

LAND USE LAND COVER CHANGE MAPPING FROM SENTINEL 1B & 2A IMAGERY USING RANDOM FOREST ALGORITHM IN CÔTE D'IVOIRE

Christian Jonathan Anoma KOUASSI¹, Chen QIAN¹, Dilawar KHAN¹, Lutumba Suika ACHILLE¹,
Zhang KEBIN¹, James Kehinde OMIFOLAJI^{2,3}, Tu YA¹, Xiaohui YANG⁴

¹School of Soil and Water Conservation, Beijing Forestry University, Beijing, China

²School of Ecology and Nature Conservation, Beijing Forestry University, Beijing, China

³Department of Forestry and Wildlife Management, Federal University Dutse, Jigawa State, Nigeria


⁴Institute of Desertification Studies, Chinese Academy of Forestry, P. O. Box 35, Yiheyuanhou, Haidian District, 100091 Beijing, China

Article History:

- received 02 March 2023
- accepted 04 March 2024

Abstract. Monitoring crop condition, soil properties, and mapping tillage activities can be used to assess land use, forecast crops, monitor seasonal changes, and contribute to the implementation of sustainable development policy. Agricultural maps can provide independent and objective estimates of the extent of crops in a given area or growing season, which can be used to support efforts to ensure food security in vulnerable areas. Satellite data can help detect and classify different types of soil. The evolution of satellite remote sensing technologies has transformed techniques for monitoring the Earth's surface over the last several decades. The European Space Agency (ESA) and the European Union (EU) created the Copernicus program, which resulted in the European satellites Sentinel-1B (S1B) and Sentinel-2A (S2A), which allow the collection of multi-temporal, spatial, and highly repeatable data, providing an excellent opportunity for the study of land use, land cover, and change. The goal of this study is to map the land cover of Côte d'Ivoire's West Central Soubre area (5°47'1" North, 6°35'38" West) between 2014 and 2020. The method is based on a combination of S1B and S2A imagery data, as well as three types of predictors: the biophysical indices Normalized Difference Vegetation Index "(NDVI)", Modified Normalized Difference Water Index "(MNDWI)", Normalized Difference Urbanization Index "(NDBI)", and Normalized Difference Water Index "(NDWI)", as well as spectral bands (B1, B11, B2, B3, B4, B6, B7, B8) and polarization coefficients VV. For the period 2014–2020, six land classifications have been established: Thick_Forest, Clear_Drill, Urban, Water, Palm_Oil, Bareland, and Cacao_Land. The Random Forest (RF) algorithm with 60 numberOfTrees was the primary categorization approach used in the Google Earth Engine (GEE) platform. The results show that the RF classification performed well, with outOfBagErrorEstimates of 0.0314 and 0.0498 for 2014 and 2020, respectively. The classification accuracy values for the kappa coefficients were above 95%: 96.42% in 2014 and 95.28% in 2020, with an overall accuracy of 96.97% in 2014 and 96 % in 2020. Furthermore, the User Accuracy (UA) and Producer Accuracy (PA) values for the classes were frequently above 80%, with the exception of the Bareland class in 2020, which achieved 79.20%. The backscatter coefficients of the S1B polarization variables had higher GINI significance in 2014: VH (70.80) compared to VH (50.37) in 2020; and VV (57.11) in 2014 compared to VV (46.17) in 2020. Polarization coefficients had higher values than the other spectral and biophysical variables of the three predictor variables. During the study period, the Thick_Forest (35.90% ± 1.17), Palm_Oil (57.59% ± 1.48), and Water (5.90% ± 0.47) classes experienced a regression in area, while the Clear_Drill (16.96% ± 0.80), Urban (2.32% ± 0.29), Bareland (83.54% ± 1.79), and Cacao_Land (35.14% ± 1.16) classes experienced an increase. The approach used is regarded as excellent based on the results obtained.

Keywords: random forest, Google Earth Engine, multispectral index, ArcGgis, land-use/land-cover change, Cote d'Ivoire.

 Corresponding author. E-mail: yangxh@caf.ac.cn

1. Introduction

Remote sensing images with very high spatial resolution (VHR) have significantly aided vegetation monitoring and mapping during the last decade, enabling for the gathering of very detailed and exact data. However, analysis of

optical data was rapidly hampered by the fact that cloud cover could be detected in the majority of images available in some parts of the earth. Understanding the location, size, and natural variability of wetlands is critical for their preservation in the face of land-use and environmental change, which is only one the reasons why (Ozesmi & Bauer, 2002).

Many applications, including natural resource preservation, sustainable development, and climate change (S. Chaudhary & Dhanya, 2018; Disse et al., 2018; Rajbongshi et al., 2018), need extensive information on LULCC at global and regional scales (A. Chaudhary et al., 2018; Dhanya & Yerramalli, 2018). Remote sensing data are often used to obtain information on land-use and land-cover (Huang et al., 2017), particularly for agricultural land. This may be performed by using high-resolution remote sensing data to generate LULCC maps, which reflect land-use for various human activities, such as agricultural or residential areas, or physical aspects of the Earth's surface such as water bodies, grasslands, and rocks (A. Chaudhary et al., 2018; Shalaby & Tateishi, 2007).

LULCC map are very useful for analyzing the composition and layout of a landscape as well as spotting changes in the landscape. They may also be used to assess modifications in the landscape caused by environmental gradient (Vizzari & Sigura, 2015). Understanding the changes in LULCC throughout the course of a study period, as well as the spatial identification of transformation hotspots, is required of measuring and spotting small changes. This data is useful for monitoring, planning, and managing ecosystems. Such classifications often need an early step in which the multitemporal images is created to minimize cloud cover and image statistics and spectral indices are produced to improve classification accuracy.

This is where GEE comes into play. It is a simple application that enables users to establish several operating modes for the combining of input data, allowing for the efficient development of a lightweight, cloud-free, multitemporal composite dataset without dealing with bottlenecks caused by restricted local processing resources (Hermosilla et al., 2018; Méger et al., 2019). When applied to remote sensing data, standard LULCC automated classification algorithms depend on the use of training data to create spectral signatures of selected land cover classes and pixel-based discrimination between diverse land-cover types (Pfeifer et al., 2012). This is why optical remote sensing data from various platforms, such as IKONOS, Quickbird, Worldview, ZY-3 (Zone 3), Sentinel, Landsat, and Moderate Resolution Imaging Spectroradiometer (MODIS), with spatial resolutions ranging from less than one meter to hundreds of meters, has been used by many researchers in a variety of research areas, including land-use classification and land-cover mapping (Congalton et al., 2014; Ghorbanian et al., 2020).

Following the successful launch of Sentinel 1A in April 2014, the ESA launched Sentinel-2, an optical satellite with high spatial resolution, on June 23, 2015. This sensor, can provide systematic worldwide captures of multispectral images with fine spatial resolution and revisit frequency (Çavur et al., 2019). This is critical for the next generation of operational products, such as land cover maps, land-use change detection maps, and geodesic variables (Pesaresi et al., 2016).

Because of its attractive properties, such as a spatial resolution of 10 m for four bands and a return length of 10

days, Sentinel-2A image are especially effective for tracking regional sensing changes over short time periods. The rich information on spectral and spatial quality allows for precise differentiation of land types. Indeed, as previously noted, multi-date satellite data is essential to reduce the uncertainty associated with land cover classification.

Sentinel-2A data have recently been provided with a higher spatial resolution than Landsat images, prompting the scientific community to choose Sentinel-2A data for their land use and land cover classification in various studies such as wetland monitoring (Kaplan & Avdan, 2017), crop and tree species classification (Immitzer et al., 2016), urban sprawl (Lefebvre et al., 2016) urban green space analysis (Kopecká et al., 2017). Several studies comparing the classification accuracy of Landsat data especially Landsat-8 and Sentinel-2A had more features than other data such as MODIS.

GEE is now one of the most commonly utilized of these systems, meeting the primary storage, composition, processing, and analysis needs of remote sensing data (Pazúr et al., 2017). This platform includes a variety of ways for LULC classification based on sophisticated algorithms. Its user-friendly interface and straightforward JavaScript language allow the developed scripts to be readily reproduced and exploited through the cloud platform. The GEE API may be used to import and visualize huge satellite photos, as well as to perform complicated geostatistical and geospatial operations on the images. Furthermore, GEE uses cloud computing to analyze data and offers a huge number of datasets from Landsat, Sentinel, MODIS, and other sensors, as well as techniques like as SVM, RF, Naive Bayes, and others. Sentinel imagery has been used in number of previous vegetation studies, including classification (Laurin et al., 2016; Perez et al., 2018; Tesfamichael et al., 2018), grassland (Mostafa et al., 2022; Sánchez-García et al., 2020), and forests (Chemura et al., 2017; Plank et al., 2019; Selvakumaran et al., 2018). In this case, the most widely used NDVI index is sensitive to vegetation characteristics (Periyasamy et al., 2021), the NDWI index is sensitive to water bodies (Qu et al., 2021) and the NDBI index is sensitive to built-up areas (Qu et al., 2021) as well as the NDMI index in order to examine their contributions to LULCC classification (Schucknecht et al., 2016). Data mining and machine learning approaches have recently evolved in the area of remote sensing to improve the performance of land cover categorization and change detection algorithms. These approaches, which are capable of coping with the complicated state and dynamics of land cover data, include neural networks, decision trees, support vector machines, RF, and ensemble classifiers.

These techniques may reach such high efficiency because they do not rely on the assumption of data distribution, but rather are capable of coping with noisy observations (L. Breiman et al., 2003; Grinand et al., 2013). Non-parametric classification techniques like k-nearest neighbour (KNN), artificial neural network (ANN), support vector machine for regression (SVR), and RF have a better ability to discriminate fairly complex land uses between

predictors and different soil classes than ML techniques like k-nearest neighbour (KNN) (Slama et al., 2021).

GEE is now one of the most commonly utilized of these systems, meeting the primary storage, composition, processing, and analysis needs of remote sensing data (Mas, 2000). This platform includes a variety of ways for LULC classification based on sophisticated algorithms. Its user-friendly interface and straightforward JavaScript language allow the developed scripts to be readily reproduced and exploited through the cloud platform. The GEE API may be used to import and visualize huge satellite photos, as well as to perform complicated geostatistical and geospatial operations on the images. Furthermore, GEE uses cloud computing to analyze data and offers a huge number of datasets from Landsat, Sentinel, MODIS, and other sensors, as well as techniques like as SVM, RF, Naive Bayes, and others (Gorelick et al., 2017).

Comparisons of supervised classification algorithms demonstrated that RF and other classification trees generated a high accuracy of 92 percent (Rodriguez-Galiano et al., 2012c). Similarly, Mansaray et al. (2019) found that utilizing satellite images from Sentinel-1A and Sentinel-2A, RF obtained overall accuracy performances of more than 95% in their research of rice mapping in China (Mansaray et al., 2019).

In other words, the accuracy of LULC estimates could be improved by a combined use of multi-source remote sensing data. Machine learning approaches optimize algorithm performance by learning the relationships between data from the data itself, using a training dataset with as much variability of the data as possible, as described by the term “universal approximations” (Lavy & Sand, 2019). In terms of prediction performance, it has been reported that the RF classification approach outperforms other classification methods such as maximum likelihood classification, SVM, and ANN (Schneider, 2012). In addition to MODIS data (Aide & Aide, 2012), Landsat data (Rodriguez-Galiano et al., 2012b; Schultz et al., 2016; Tatsumi et al., 2015), digital soil mapping (Grimm et al., 2008), and forest biomass mapping (Baccini et al., 2012).

Throughout 1960 and 2017, Côte d'Ivoire's forest cover decreased from 12 million hectares to less than 3 million hectares, owing mostly to improved agricultural productivities, particularly cocoa and palm oil farming. Deforestation is occurring at an alarming rate, averaging about 3% each year. If current trends continue, Côte d'Ivoire's forests will soon be unable to fulfill their ecological responsibilities, harming the country's agricultural industry and jeopardizing the livelihoods of millions of small-scale farmers.

Deforestation in agricultural tropical nations is mostly caused by cocoa and oil palm crops. They a land-use system that dominates and changes most forest land use system that dominates and changes most forest landscapes in West Africa, including Ghana, Nigeria, Cameroon, and Côte d'Ivoire (Sonwa et al., 2017; Wessel & Quist-Wessel, 2015).

Indeed, previous research on deforestation in Côte d'Ivoire have provided important information on the

country's vegetation state (Abu et al., 2021); and degradation due to agriculture (Abu et al., 2021; Barima et al., 2016; Kouakou et al., 2020). However, only a few studies have investigated the use of current satellite data as sentinels (Kouassi et al., 2021c). Their work, on the other hand, is still limited in terms of object-based pixel detection modification design principles understanding and comprehension. The goal of this research is to categorize the study area by utilizing a combination of Sentinel 1B and 2A data, spectral indices, and biophysical parameters gathered during the study period.

2. Methods

2.1. Study area

This study was conducted in Côte d'Ivoire, a West African country located on the African continent between 4- and 11-degrees north latitude and 2- and 9-degrees west longitude. Côte d'Ivoire has a tropical and humid climate. The following are the country's major climatic zones: The southern hemisphere has a tropical equatorial climate. During this time of year, temperatures range from 21 °C to 33 °C (Falk et al., 2016). The weather is oppressively hot and dry. Côte d'Ivoire's two most major vegetation zones are forest in the south and savannah in the north. Because of the Southwest's climate, vegetation, and soils, tropical cash crops like as cacao and palm oil flourish (Falk et al., 2016). These two crops are crucial to the growth of the Ivorian economy. Côte d'Ivoire is now Africa's biggest palm oil exporter, accounting for 60% of total ECOWAS palm oil exports. The nation also supplies crude and refined petroleum to the regional market (Cheyng et al., 2000). In terms of cocoa output, Cote d'Ivoire is the world's leading producer, owing to the performance of massive plantations via forest exploitation, which is based on the country's vast exploitation of forest resources (Tano, 2012). The bulk of the primary woods found in the research region are home to some of the area's most biologically important ecosystems (N'Guessan et al., 2019; Sanial et al., 2023). The area (Soubré) has a diverse terrestrial vegetation, including mangroves, shrubs, and woodlands, as well as a variety of fauna and terrestrial reptiles (Assi & Guinko, 1996; Klopfer et al., 2012). The majority of recent growth activities in the region, such as major infrastructure and investment projects, are directly or indirectly linked to environmental degradation. There are also industrial palm producing companies present.

This area of the Cote d'Ivoire was selected for research because it is a crucial location for the development of industrial cash crops, as well as the biggest supplier of cocoa beans and a significant oil palm producing area. Figure 1 presents the study area.

2.1.1. Google Earth Engine tool

The GEE engine was used in this study. It is a cutting-edge cloud-based platform for geospatial and remote sensing data processing. GEE provides access to a database

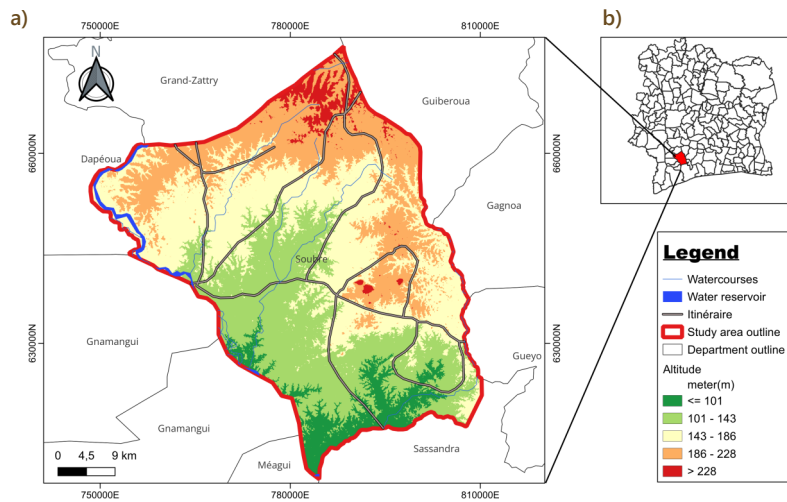


Figure 1. a – Map of the study area; b – Côte d'Ivoire map

of public remote sensing images, including Sentinel-1A and 2B, Landsat-8, and MODIS, as well as a range of extra composite products. GEE offers a Google computing infrastructure (<https://developers.google.com/earth-engine/>) to developers for parallel processing of geographic data using the Javascript API. Random Forest, Nave Bayes, Classification And Regression Trees (CART), and Support Vector Machine (SVM) are just a handful of the machine learning algorithms for classification available on the GEE platform (Mohammadi & Khodabandehlou, 2020).

2.1.2. Data

Sentinel imaging data has been widely employed in land use classification, environmental monitoring, and urban planning, as well as in the assessment of LULCC. The Sentinel-1 synthetic aperture radar (SAR) and Sentinel-2B cloud-free multispectral images used in this study were available from the ESA Copernicus Sentinel Scientific Data Hub (<https://scihub.copernicus.eu/dhus/#/home>). The Sentinel-1A C-band images utilized in this study were captured in the wide swath interferometry mode of both the VH (vertical emission – horizontal reception) and VV (vertical emission – vertical reception) polarizations of the VH (vertical emission – horizontal reception). The SAR images have a pixel size of 10 m and are processed at the greatest resolution possible, Ground Range Detection (GRD) level 1. Because of its architecture, the sensor onboard this satellite can gather data at a frequency of 5405 MHz and in a range of polarizations (European Space Agency, 2019). Sentinel-2B top-of-atmosphere reflectance images recorded at Level 1C were utilized in this investigation, and they were orthorectified and spatially registered following processing. The imaging had a resolution of 10 m (bands 2–4 and 8), 20 m (bands 5–7, 8a, 8b), and 20 m (bands

5–7, 8a, 11–12), and 60 m (bands 5–7, 8a, 11–12) in the visible and near-infrared areas, and a resolution of 10 m (bands 5–7, 8a, 11–12) in the shortwave infrared region (band 1, 9–10).

2.2. Processing








Using the GEE platform, we were able to access Sentinel-1A and 2B multi spectral radar (MSR) data by filtering the data for the region of interest, which was the study area. To cover the whole satellite image, about 1740 training polygons were physically scanned in the study area, and samples were collected at random. The training sample specifically comprises seven distinct kinds of land cover and land use classifications: The categories are as follows: (1) Thick Forest; (2) Urban; (3) Clear_Drill; (4) Cocoa_Land; (5) Water; (6) Bareland; and (7) Palm_Oil. The survey findings are shown in Table 1. This technique ensures that a representative sample of each terrain type is used (Wang et al., 2019). It is feasible to improve the accuracy of the most accurate classification in non-parametric machine learning classification, such as RF, by using a large number of reference data (Chrysafis et al., 2017). The test polygons were divided in half so that they could be utilized for both testing and validation. Among other things, this resulted in the construction of 1740 training polygons, 870 training polygons, and 870 test polygons. We manually labeled high-resolution Google Earth images between 2014 and 2020 that we received from the Internet. After that, we utilized visual verification to ensure that the supplied class was accurate. Table 2 shows the defined land cover classes that have been selected.

The images were then imported into GEE for additional processing (Murray et al., 2018). The GRD bands were

Table 1. Class training point

Class	Thick_Forest	Urban	Clear_Drill	Palm_Oil	Water	Bareland	Cocoa_land	Total
Validation training Point	212	255	225	205	265	207	371	1740

Table 2. Land Categories definition (W. Li et al., 2020; Xiong et al., 2017)

Land Classification	Class colors	Définition
Thick_Forest		*Forest, natural or planted forests, evergreen forest land, mixed forest land.
Urban		*Built-up area of all settlement, including industrial zones and other artificial surfaces.
Clear_Drill		*Deciduous forest land, Shrubs or herbaceous may be present.
Palm_Oil		*Industrial and traditional oil palm plantation.
Water		*Lakes, rivers, marries, wetlands, reservoirs, streams and canals, reservoirs, bays, estuaries.
Bareland		*Bareland, exposed rock, strip mines, quarries, gravel pits, transitional areas, mixed barren.
Cocoa_Land		*Industrial and traditional cocoa plantation.

eliminated and the noise was corrected before processing the S1 image; radiometric correction and terrain correction were performed using the orbit file, which was then applied to the S1A image (Gulácsi & Kovács, 2020; Veci et al., 2014). The S1 data were filtered to obtain “transmitterReceiverPolarisation” [“VV” and “VH”] and “filterMetadata” to obtain “instrumentMode”, “equals”, and “IW” (Khan et al., 2020). The S2B images were pre-filtered to get less hazy granules and to reduce the number of cloudy pixels to 20% of the overall image. Additionally, the S2B data was filtered using the pixel quality characteristics of the “Pixel QA” band as defined by the CFMaskAlgorithm, which was applied to the S2 data.

The clouds were removed using the “Pixel QA” band, which is a binary mask band with a CFMask quality indicator (CFMask) (Foga et al., 2017). Bits 10 and 11 in the visualization represent S2’s cloud shadow, and are referred to as the “CloudBitMask” and “cirrusBitMask”, respectively, as well as the Masks [qa.bitwiseAnd (cloudBitMsk)] and [qa.bitwiseAnd (cirrusBitMask)]. These filter functions were used to minimize speckle noise (an extremely noisy, salt-and-pepper look), which reduces image quality and hinders image interpretation (Choi & Baraniuk, 2001; Fosgate et al., 1997). The benefit of this technique is that it makes use of the intensity data as well as the intrinsic pixel structure of the SAR data (Amitrano et al., 2014; Gao et al., 2017). The function “updateMask” was created by multiplying the bands from 1 to 11 by a factor of 10000. A backscatter coefficient was derived using S1 data on the “VV” data, and bands 8, 4, and 3 were used as false colours on the “VV” data.

To collect data across the region of interest, the interferometric wide swath mode (IW) was used. The Terrain Observation with Progressive Scan SAR (TOPSAR) approach is utilized in the IW mode to acquire three sub-sweeps. This approach gathers data in pulses by cyclically switching the antenna beam between the three sub-bands. The main indices were computed and the results were compared to each other for feature classification prediction. In order to identify which predictor was the most successful, GINI was used to assess the importance of the S1A and S2B features, as well as the properties of the spectral bands and vegetation indices.

The GINI coefficient was chosen because it provides an idea of the average total diminution of the impurity of the nodes, and because it was applied to all of the RF decision trees. GINI feature provided us with information on how important the input characteristic was relative to the

classification (Argamosa et al., 2018; Descals et al., 2019; Han & Lee, 2020; Mansaray et al., 2020). The sample point was performed to develop the categorization of S1A and S2B with RF. In this research, we looked at the producer accuracy (PA), user accuracy (UA), and Kappa accuracy coefficients (KA). In the last step of the categorization process, the land cover maps were converted into polygonal shape files in ArcGIS for subsequent processing and analysis.

2.2.1. Accuracy assessment

The accuracy assessment was created to assess a model’s ability to detect and define land use and land cover categories in a study area. In the accuracy assessment, it quantifies the accuracy of the maps, calculates the area of each class formed by the reference classification, and analyses the uncertainty of the classifications of the area classifications (Olofsson et al., 2014). The validation score approach, which was used to validate the RF model, was used to assess the correctness of the RF model. The validation score is calculated by reserving a part of the original training data before training the models and then evaluating the models’ efficacy using ensemble decision trees (Sharma et al., 2020).

The classification accuracy was expressed in terms of the estimated confusion matrix in terms of overall accuracy, error of commission (user accuracy), and error of omission (omission error) (producer accuracy). The matrix’s column contains the reference information, the row has the classification result information, and the intersection of the two columns produces the number of samples classified in a certain class (Rodriguez-Galiano et al., 2012a). In general, overall accuracy refers to the percentage of correctly categorized samples, while user accuracy refers to the proportion of correctly identified samples in each class. We utilized a slightly modified version of the technique described by (Olofsson et al., 2014) to assess the accuracy of the land cover. This research used a stratified random sampling method. By applying the following formula to the data, the proper sample size was calculated (Olofsson et al., 2014) Equation (1):

$$n = \frac{\sum (w_i s_i)^2}{\left[s(\hat{\theta}) \right]^2 + \left(\frac{1}{N} \right) \sum (w_i s_i)^2} \approx \left(\frac{\sum (w_i s_i)^2}{s(\hat{\theta})} \right), \quad (1)$$

where n = the number of units, $s(\hat{\theta})$ is the standard error of the estimated overall accuracy,

W_i is the mapped percentage of the area in class i and S_i is the standard deviation of the mapped proportion of the area in class i Equation (2):

$$S_i = \sqrt{U_i(1-U_i)}. \quad (2)$$

Different Accuracies (User's, Producer's, Overall and Kappa coefficient) have been calculated for verifying the time-series RF classification (Ghosh et al., 2014).

2.2.2. Random Forest classification method

It is a robust model, well-suited to classification, and it can cope with both a large number of predictor variables and large and difficult data sets with reasonable ease (Cutler et al., 2007; Kolyaie et al., 2019). Amit and Geman (1997) developed a CART approach that iteratively constructed a large CART cluster by combining bagging (R. F. Breiman et al., 1990; Amit & Geman, 1997) with random variable

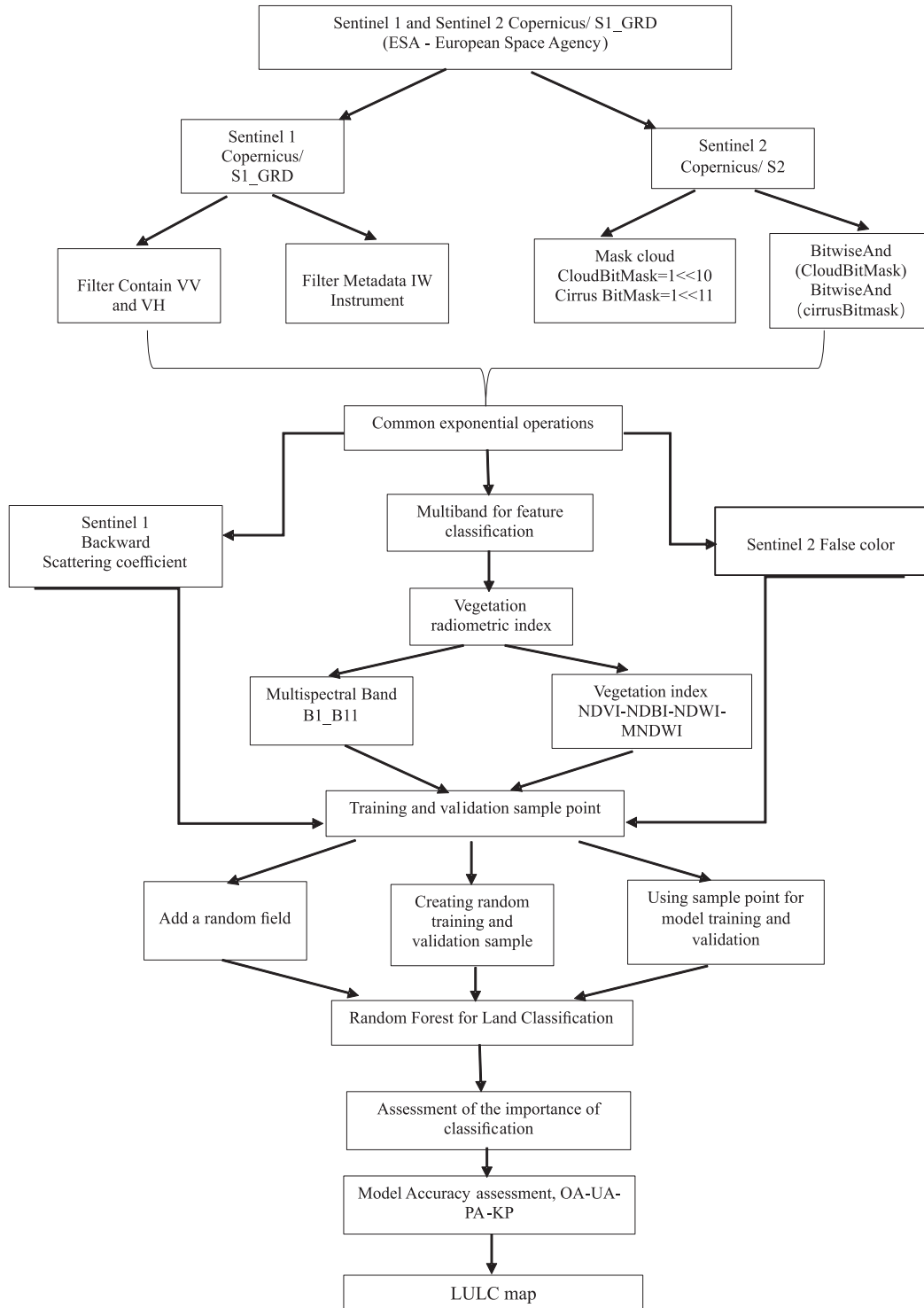


Figure 2. Flow chart of the steps used for land use and land cover mapping using Sentinel data and multispectral imagery with RF implemented in GEE and AcrGIS 10.7

selections at each node (Amit & Geman, 1997; R. F. Breiman et al., 1990). The classification result represents a majority vote or an average of the data in the collection. Without the necessity for pruning, each internal node of a number of RF decision trees determines the appropriate separation features from a randomly chosen sample of predictors (Dhanda et al., 2017; G. Li et al., 2019); RF, which is based on the bootstrap sampling approach, ensures that the minimum possible bias and data variance are attained (Jović et al., 2012). Table 3 describes the satellite data features for preparing sentinel and predictor data. Figure 2 show the workflow of this study.

2.2.3. Choices of indices

Sentinel-2B bands 4 and 8, which correspond to Near InfraRed (NIR) and red wavelengths, respectively, were used to forecast vegetation in a number of calculations, including the NDVI. Bands 3 and 8, which correlate to NIR and green, were used to develop the NDWI. Bands 3 and 11 of the MNDWI were used as prediction variables, whereas bands 8 and 11 of the NDBI were used as prediction variables. Finally, the GEE “maskS2clouds” function was used to the S2B images, together with the “CloudBitMask” and “CirrusBitMask” variables, to mask any cloud interference and provide a median composition per pixel for each of the multispectral bands and each of the four indices, respectively. Because of the employment of these approaches, it was feasible to eliminate from the final composite image dark pixels generated by shadows as well as unnaturally bright pixels caused by lingering clouds. Table 4 shows the Sentinel imagery that was obtained for the research.

Table 4. Sentinel data images used for this study

Mission (2014–2020)	Product	Cell Size (m)	Agency
Sentinel-1B	Level-1 GRD-HR	10	ESA/Copernicus
Sentinel-2A	Multispectral image Level-1C	10	ESA/Copernicus

3. Results

Sallustio et al. (2015) showed that the Confusion Matrix (CM) result is a common approach for evaluating the categorization accuracy of remote sensing images (Sallustio et al., 2015). Overall, the UA and PA coefficients are more than 90% for the years 2014 and 2020, with the exception of two years in which the PA was less than 90%, which happened in the Bareland class in 2014. The most favoured years were 2014 (81.90%) and 2020 (79.20%) (Tables 5 and 6). The success of the strategy was shown by the highest possible scores obtained across all courses. When comparing the PA and UA of the Clear Drill, Water, and Palm Oil classes in 2014 to the other soil classes, the RF classifier considerably overestimated the PA and UA of the Clear Drill, Water, and Palm Oil classes in 2014. It did, however, drastically underestimate the PA and UA of the 2020 Bareland class

The Table 7 includes the coefficients, overall accuracy, and kappa values. The figures for 2014 are higher than the values for 2020, and they account for more than 95 percent of the total.

Figures 3 and 4 show the UA and PA values for the soil types in 2014 and 2020, respectively. As a result of

Table 3. Sentinel data preprocessing and predictors

Imagery data	Predictors	Predictors of Interest	Description	References
Sentinel-1	Polarization	VV	vertical transmit-vertical channel	
		VH	vertical transmit-Horizontal channel	Chen et al. (2023)
		V/H	VV/VH	
		VH-VV	transmitterReceiverPolarisation	
	Texture	VH+VV	transmitterReceiverPolarisation	Haifeng et al. (2020)
		IW	instrumentMode, equals	
		B1	Ultra Blue, 443 nm	
Sentinel-2	Multispectral bands	B2	Blue, 490 nm	
		B3	Green, 560 nm	
		B4	Red, 665 nm	https://gisgeography.com/
		B6	Red edge, 749 nm	
		B7	Red edge, 783 nm	
	Vegetation Indices	B8	Near Infrared, 842 nm	
		B11	Short Wave IR, 1610 nm	
		MNDWI	(Band 3 – Band 11)/ (Band 3 + Band 11)	Chen and Zhao (2020)
		NDBI	(Band 11 – Band 8)/ (Band 11 + Band 3)	Mengqi et al. (2022)
	Vegetation Indices	NDWI	(Band 3 – Band 8)/ (Band 3 + Band 8)	Pattanayak and Diwakar (2018)
		NDVI	Band 8 – Band 4)/(Band 8 + Band 4)	C. Huang et al. (2021), Jiaxin et al. (2023)

Table 5. RF confusion Matrix results 2014

Class	Thick_Forest	Urban	Clear_Drill	Palm_Oil	Water	Bareland	Cocoa_land	Commission	Omission	PA
Thick_Forest	154	0	1	0	0	0	1	0.012	0.083	91.66±1.87
Urban	0	125	0	0	0	3	1	0.018	0.031	96.89±1.92
Clear_Drill	0	0	111	4	0	0	3	0.212	0.005	94.06±1.91
Palm_Oil	0	0	0	101	0	4	4	0.198	0.009	92.66±1.95
Water	0	0	0	0	131	0	0	0	0	100±1
Bareland	14	4	1	0	0	81	1	0.246	0	81.90±1.77
Cocoa_land	0	0	4	1	0	5	194	0.025	0.015	95.09±1.93
Total	168	129	117	106	131	93	204	-	-	-
UA	89.43±1.85	96.84±1.92	94.87±1.93	95.28±1.90	100±1	87.09±1.94	95.09±1.93	-	-	-

Table 6. RF confusion Matrix results 2020

Class	Thick_Forest	Urban	Clear_Drill	Palm_Oil	Water	Bareland	Cocoa_land	Commission	Omission	PA
Thick_Forest	148	0	2	4	0	0	2	0.013	0.081	94.87±1.90
Urban	1	124	0	0	0	5	0	0.023	0.032	95.12±1.95
Clear_Drill	0	0	111	2	0	0	3	0.02	0.054	94.87±1.90
Palm_Oil	3	0	0	100	0	2	2	0.0129	0.029	93.47±1.94
Water	0	0	0	0	131	0	0	0	0	100±1
Bareland	11	4	2	3	0	80	1	0.259	0	79.20±1.74
Cocoa_land	1	0	4	5	0	3	194	0.025	0.025	93.71±1.93
Total	164	128	119	114	131	90	202	-	-	-
UA	90.24±1.87	96.87±1.92	93.27±1.90	87.71±1.87	100±1	88.88±1.95	97.48±1.93	-	-	-

Table 7. Comparison of Overall and Kappa accuracy of two classifications

Accuracies	2014	2020
Kappa	96.42±1.92	95.28±1.91
Overall	96.97±1.93	96±1.92

the classification approach adopted, better results were achieved in both study years. Except for the Bareland class for the year 2020, the average accuracy ratings are around or over 90%. In general, accuracy is falling in 2020, compared to the accuracy levels obtained for the PA created the previous year. Some categories, however, such as the water class, have remained stable.

When the findings of Figures 3 and 4 are compared, it is clear that the backscatter coefficients VV (46.17) and VH (50.37) of S1 for 2014 have much higher values than the other predictor variables. The NDWI (51.01) and Sentinel variables are determined to be the strongest predictors among these three prediction categories, followed by spectral B1 (49.59), B11 (47.56), and B3 variables (44.99). The backscatter coefficient value (70.81) is higher than the other predictors in the Sentinel-1 VH polarizations. The VV polarizations show greater values than the other predictors, as do the spectral index B2 (57.98), NDWI (56.75), and NDBI (53.21). NDVI has decreased in all variables except the cross-polarization backscatter coefficients VH (70.80

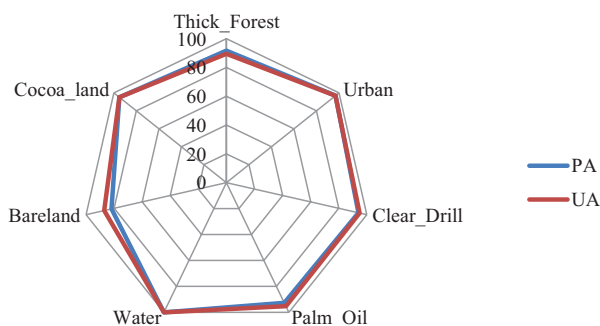
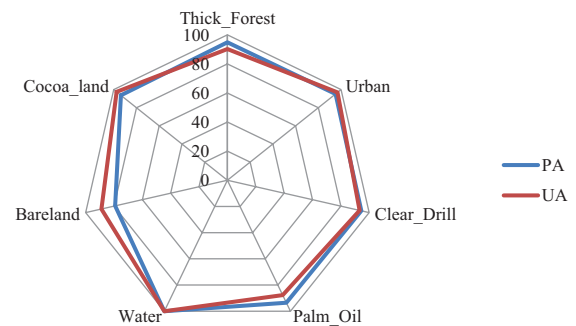
**Figure 3.** LULCC producer and User accuracy in 2014**Figure 4.** LULCC producer and User accuracy in 2020

Table 8. Importance of GINI of Number tree 2014

Indices	B1	B11	B2	B3	B4	B6	B7	B8	MNDWI	NDBI	NDVI	NDWI	VH	VV
Values	51.55	50.18	57.98	44.11	50.12	47.20	43.91	44.30	56.75	53.21	47.20	48.29	70.80	57.11

Table 9. Importance of GINI of Number tree 2020

Indices	B1	B11	B2	B3	B4	B6	B7	B8	MNDWI	NDBI	NDVI	NDWI	VH	VV
Values	49.59	47.56	42.49	44.99	36.54	32.25	31.48	32.45	45.95	46.60	34.34	51.01	50.37	46.17

for 2020) and VV (54.11 for 2021) (Figures 5 and 6), both of which are substantially related to NDVI. Furthermore, we notice a reduction in the importance of NDWI from 51.01 to 48.29 for the years 2014 and 2020, indicating a decrease in moisture of NDVI from 34.34 to 47.28, indicating a decrease in moisture (Tables 8 and 9).

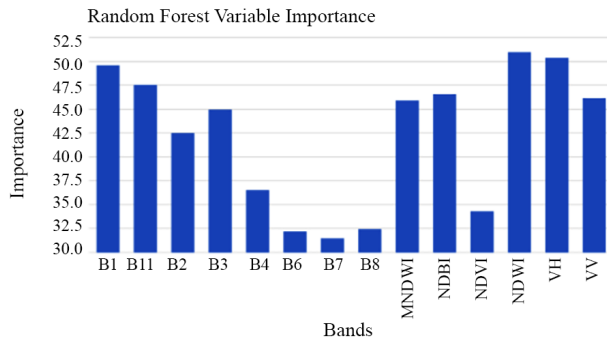


Figure 5. Variable importance of Gini feature histogram showing the relative contribution of the top 14 most influential predictor variables (2014)

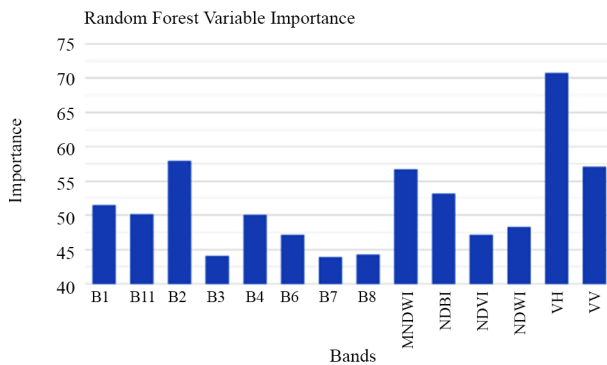


Figure 6. Variable importance of Gini feature histogram showing the relative contribution of the top 14 most influential predictor variables (2020)

3.1. LULCC analysis

Following the categorization results, an assessment of change detection was performed in order to identify the evolutionary tendency of the different classes studied within the study area. We were able to finish the LULCC categorization inquiry using the ArcGIS 10.7 platform (Rosan et al., 2021). Using the pixel-based categorization result images, the total area and change of each LULCC

were computed. Calculations were carried out to determine the total area and change of each LULCC class within the study’s area. The formulae Equations (3–4) were used to calculate the total area and change of each LULCC class in the study area from these pixel-based classification result images for the purpose of change detection, and the formula Equation (5) was used to calculate the rate of change in the study area from 2014 to 2020 from these pixel-based classification result images. The proportion of each LULCC type used was calculated using the following formula:

$$S_i\% = \frac{S_i}{S_t} \times 100\%; \tag{3}$$

$$S_i = S_{it_1} - S_{it_2}; \tag{4}$$

$$S_{ir} = \left[\frac{S_{it_1}}{S_{it_2}} - 1 \right] \times 100\%, \tag{5}$$

where S_i denotes the land use type area, “ i ” S_t denotes the total study area, and S_i percent denotes the proportion of each land use type area in the overall research area. S_{it_1} and S_{it_2} refer to the total area of land use type “ i ” in the first and second years of the land use type “ i ” categorization system, respectively (Alam et al., 2020). In this study, the word “area” refers to the rate of change, which is the magnitude of change observed between 2014 and 2020 (Tian et al., 2014). Table 10 shows the change in surface area for each of the soil classifications assessed. Figure 7 shows the proportions of changes in land cover and use.

Table 10. LULCC area percentage and change rate for 2014 and 2020

Class	Area (Km ²) in 2014	Area (Km ²) in 2020	Net LULC change (Km ²)	Percentage (%)
Thick_Forest	47 656.55	35 066.13	-12 590.13	35.90±1.17
Urban	2166.3	2218.82	+55.52	2.32±0.29
Clear_Drill	84 343.88	101 577.79	+17 234.91	16.96±0.80
Palm_Oil	23 878.98	15 152.46	-8726.52	57.59±1.48
Water	3119.52	2951.70	-162.82	5.90±0.47
Bareland	1935.17	11 755.17	+9824	83.54±1.79
Cocoa_Land	21 258.98	32 912.31	+11 654.33	35.14±1.16

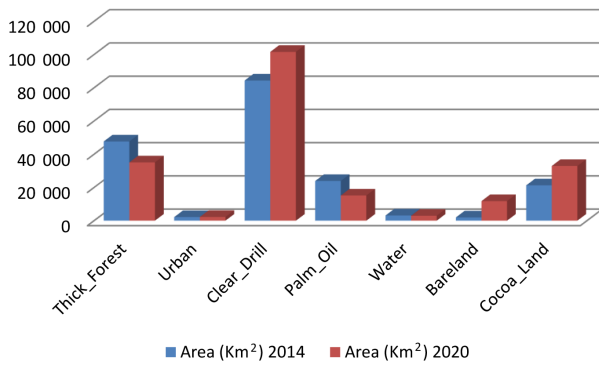


Figure 7. Land-use/land-cover area loss and gain between 2014 and 2020

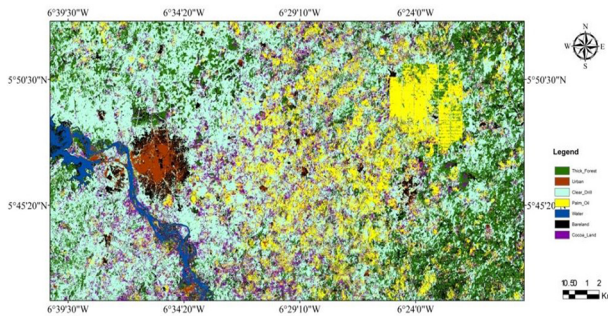


Figure 8. RF LULCC classification map of study area in 2014

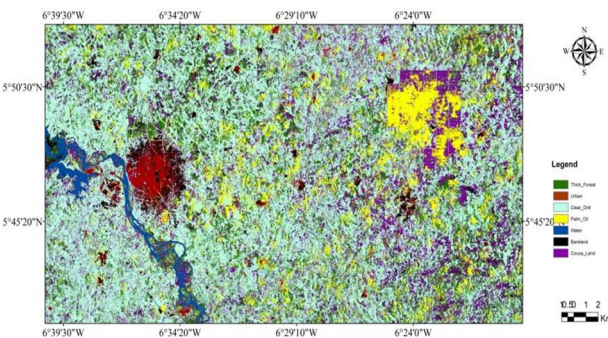


Figure 9. RF LULCC classification map of study area in 2020

4. Discussion

4.1. Sentinel classification

We were able to determine the GINI Importance of Tree Numbers values for fourteen distinct types of spectral indexes using pre-processed S1A and S2B images (Tables 7 and 8). Many previous research has shown that many remote sensing and vegetation indicators are sensitive to different types of LULCC (V. F. Rodriguez-Galiano et al., 2012b). As a result, the approach used in this study, which was based on a combination of remote sensing and vegetation spectral indexes, was effective in discriminating between the various types of vegetation observed in the analyzed area (Aredehey et al., 2018; Atzberger, 2013; Pareeth et al., 2019; V. F. Rodriguez-Galiano et al., 2012c). Previous study found that when comparing the coefficients of

the Sentinel spectral indexes and the vegetation indices, as well as the relevance of GINI characteristics in RF, the Sentinel-1A texture features showed a high potential for predicting the categorization of LULCCs (Bourgoin et al., 2021). Backscatter coefficient values of parallel cross-polarizations in 2014 are higher (VH: 70.80; VV: 57.11) than in 2020 (VH: 50.37; VV: 46.17) and greater than the other plant and spectral index values. Overall, the values for 2020 are significantly higher than those for 2014. Overall, these biophysical vegetation characteristics, as well as the Sentinel-1A data polarization variables, were extremely valuable for land categorization.

Indeed, as previous research has shown, the S1A backscatter coefficient and the S2B vegetation indices were effective and frequent predictors. The C-band backscatter "VV" is very sensitive to soil moisture in open areas (Nonni et al., 2018), and it has been found to be useful in distinguishing the different types of vegetated or herbaceous land covers in the study area (crop, Thick Forest, Clear Drill, Water bodies) (Aleksiev & Chernikhovskii, 2021; Khellouk et al., 2021). In the study field, a method based on a combination of remote sensing spectral indices, biological variables, and backscatter coefficients was created and tested, and it was shown to be effective in identifying LULCC and change detection. The spatial resolution of the Sentinel-1A and Sentinel-2B data revealed its use in categorizing features in the area, showing the data's significance. It was discovered that change detection by LULCC classification was effective, with good accuracy values for the PA and UA coefficients, as well as the OA coefficients, using the method of combining biophysical variables, backscatter coefficients from S1A and S2B images, and remote sensing spectral indices.

According to various authors, classifications are inaccurate when vegetation is characterized by spatial complexity (Garioud et al., 2021). Despite the complexity of the study area, the extra spectral bands of Sentinel-2A were crucial in boosting the identification and mapping of the plant cover in the study area, as shown in this work. The findings revealed significant differences at the class level, with both losses and gains in area observed. The random forest approach, which was implemented in GEE, was used to successfully categorize land uses. As a consequence, we may infer that the combination of a high spectrum resolution and a reasonably excellent spatial resolution at S1A & S2B allowed the RF classification to yield superior classifications, with an out-OfBagErrorEstimate of 0.0314 in 2014 and a value of 0.0498 in 2020.

Thus, the interplay of spectral indexes with biophysical parameters and polarization variables was critical in the development of an image that contained all three types of information and was capable of discriminating and categorizing the different characteristics with high accuracy. The images from S1A and S2B may have made a substantial contribution, notably in distinguishing soil types. The biophysical variables of parallel and

cross polarization of S1A (the “VV” and “VH” of S1), spectral indices, and vegetation indices, among others, might be used to identify the distinct classes present in a mixed pixel. Classifications that were valid and generated greater accuracy characteristics were created using Sentinel-1A and 2B data, as well as polarization and backscatter variables. The spectral bands used in this study, which included the B1, B2, B3, B4, B6, B7, B8, and B11 bands, provided a substantial amount of value to the biophysical indicators, allowing for more accurate distinction between classes and better categorization. Indeed, these differences are particularly important when it comes to classifying more complex creatures such as mammals (Radoux et al., 2016). Aside from that, a combination of the spectral bands B3 to B11, as well as the spectral bands 7 to 8, and B11, proved to be very intriguing in the classification of agricultural areas (Palm-oil and Cocoa), as it was capable of discriminating between the various crops.

Authors were able to distinguish between the different classes with greater accuracy ratings because to the technique adopted in this investigation, which incorporated spectral and biophysical characteristics from S1A and S2B multispectral optical imaging data. Figures 8 and 9 show a multi-date colour composite in “VH” polarization of the radar backscatter coefficient for the years 2014 and 2020, respectively, based on the radar polarimetry characteristic of the Sentinel data used. Each of these distinct colours signifies a change in phenology at various plant stages during the duration of the study period’s seasons. In Côte d’Ivoire, four distinct seasons are recognized and recorded, during which certain vegetation loses its greenness or changes colour and wilts depending on whether it is the dry or rainy season, but the bulk of forest areas remain their dominant colour, which is green.

The reason for this is because the cross-polarized backscattered signal and the sensor signal are distinct, and the sensor signal contains or maintains information about the radar response, as shown in our sentinel-1 data. The radar images captured in our case using various combinations of spectral, polarization, and wavelength variables in cross-polarization “VH” were thus able to detect changes in the classes and provide different and complementary information on the various classes over the course of the study period. When RF classification was applied to S1A and S2B data (Figures 8 and 9), the overall classification accuracy improved. According to the confusion matrix, the overall accuracy for 2014 and 2020 is 96.97% and 96%, respectively, which is rather impressive for a prediction system.

The Kappa coefficient was calculated using the information provided by the matrices. The kappa value of 96.42% and 95.28%, respectively. A value of greater than 90% was obtained for practically all of the classifications studied, including “Thick Forests”, “Urban”, “Clear_Drill”, “Palm_Oil”, “Water”, “Cocoa_Land”, and “Bareland”, suggesting that the overwhelming majority of pixels were

appropriately recognized. On the contrary, with the exception of the class “Bareland”, which earned a value less than 90 percent (81.90%) and (79.20%) for the years 2014 and 2020, all other classes received values lower than 90 percent. According to the commission error, which is the proportion of pixels that are classified in a different class than the one to which they should belong (Collet & Calloz, 2001), in 2014 the class “Thick_Forest” had 2 pixels wrongly classified, Clear_Drill class had 7 pixels, Urban had 4 pixels, the class “Palm Oil” had 8 pixel, the class “Bareland” had 20 pixels, and the class “Cocoa_Land” had 10 pixels. In 2020, the class “Thick Forest” had 8 pixels incorrectly classified, Urban had 6, the class “PamI_Oil” had 7 pixels incorrectly classified, the class “Bareland” had 21 pixels incorrectly classified, and the class “Cocoa Land” had 13 pixels incorrectly classified, “Clear_Drill” had 5 pixels incorrectly classified; in total, 60 out of 888 pixels do not belong to these classes. With the classification technique applied in this analysis, the overall RF performance may be classed as good, notwithstanding the misattributed pixel identified in this study.

4.2. The influence of agricultural on biodiversity

Cote d’Ivoire is a developing nation whose economy focuses on agriculture (export crops) and primary industries, particularly mining, which constitute the vast majority of its economic production and income (Eveillé et al., 2020).

According to Kouakou (2021), basic crops such as cocoa, oil palm, and coffee are the key sources of economic income in Côte d’Ivoire, as well as the biggest land consumers (Kouakou, 2021). Over the past three decades, these crops have been recognized as contributors of deforestation in the nation (Kouassi et al. 2021a, 2021b; Assalé et al., 2020; Ruf et al., 2020; Ruf & Varlet, 2017). According to World Bank estimates, agriculture has contributed more than three-quarters of total GDP in every year from the country’s independence to the present (Ongolo et al., 2018). It is the most significant source of employment and income for around two-thirds of the country’s citizens, accounting for a quarter of the total.

This understanding may explain the significant pressure that has been imposed on forest area by increasing export crops in order to fulfill agriculture as the country’s principal economic resource. Figure 9 depicts the types of change, with the Bareland land class having the highest percentage of change (83.54%), followed by the Palm Oil land class, and the Thick_Forest land class having the lowest percentage of change (70%). The losses and increases on both sides of the land cover classes over the study period indicate a change in the study area. Our results back with the findings of Global Forest Watch, which predicted that Côte d’Ivoire would lose around 248,000 hectares of primary forest by 2020. A substantial percentage of this deforestation is caused by the clearance of forest for plants used in the global cocoa business. The loss of

Thick_Forest area was equal to the loss of cultivated cocoa land, according to the study's findings in Table 9. According to some ideas, this is because virgin land in the Thick_Forest class has been converted to cultivated Cocoa_land.

5. Conclusions

This study allowed us to map the study area using the pixel classification approach, which integrated biophysical characteristics, polarization variables from S1A and S2B data, vegetation indices, and spectral indices across a six-year time series. When it comes to identifying changes and categorizing the study area, the classification findings demonstrate that the combination approach based on the combination of polarization coefficients, backscatter coefficients, biophysical factors, and spectral bands proved to be quite effective. Because of the study's high spatial and temporal resolutions, the new Sentinel-1A satellite image series was found to be particularly beneficial for monitoring temporal detection change and discriminating land cover categories in the study area. Sentinel 2B was also proven to be efficient in discriminating between planted Cocoa land and palm oil. The inclusion of the cross-polarization variables "VH" in the study area classification proven to be highly important and trustworthy. The polarization variables "VV" and "VH", which had the best backscatter coefficients, were the greatest predictors of backscatter coefficients over a two-year period. These findings highlight the value of NDVI, NDBI, and NDWI indices as factors for a wide range of applications, including monitoring vegetation health, calculating farmed areas, measuring urban development, and identifying water features. In summary, this study investigates the feasibility of employing a mix of vegetation, built-up, and water indices generated from Sentinel 1 and 2 bands to aid in the mapping of vegetated areas, urban areas, and water bodies. The integration of the four data kinds (Sentinel-1, Sentinel-2, spectral indices, and biophysical indices) enhanced and accomplished excellent multi-sensor classification accuracy of the recognition for LULCC mapping by assuring exceptional multi-sensor classification accuracy. The combination of Sentinel-1 and Sentinel-2B images yielded an excellent land cover classification accuracy of more than 90%. SAR data features from Sentinel 1A that included several temporal and polarization bands aided in distinguishing across data classes. With the aid of this study, we will be able to follow the LULCC of the main land classes in the study area through time. The findings provide light on the temporal dynamics of these spectral indices, emphasizing their critical importance in efficient land management, fostering sustainable urban growth, improving environmental monitoring, and managing water resources sustainably. In light of these findings, it is suggested that government agencies and policymakers fund new research initiatives that focus on these indices in combination with environmental concerns. This technique would help us better comprehend

changes in land use patterns, particularly in urban and agricultural regions. Furthermore, future study studies must account for the impact of elements such as fast population expansion, landscape changes, and socioeconomic variables. These factors will surely help to inform decision-making and planning for sustainable development and environmental conservation of natural resources.

Funding

National Natural Science Fund Project for International and Regional Cooperation and Exchange "Sino-Argentinian Cooperation Research on Temperate Grassland Degradation: Current Status Assessment and Recovery Strategies" (32061123005) and National Natural Science Fund Project "Joint Species Distribution Model Based Grassland Degradation Assessment and Potential Risk Projection in Hulun Buir Steppe" (41971061).

Author contributions

Ideally, people who contributed to the work are listed in this section along with their contributions conceptualization (YX) and (ZK); methodology (CJAK); software (CJAK) and (CQ); validation (YX) and (ZK); formal analysis (CQ); investigation (DAK), (TY), (LSA); data curation (JKO) and (LSA); writing—original draft preparation (CJAK); writing—review, and editing (CJAK); visualization (DKA) and (JKO), (TY); supervision (YX) and (ZK); project administration (YX); funding acquisition (ZK). All authors have read and agreed to the published version of the manuscript.

References

- Abu, I.-O., Szantoi, Z., Brink, A., Robuchon, M., & Thiel, M. (2021). Detecting cocoa plantations in Côte d'Ivoire and Ghana and their implications on protected areas. *Ecological Indicators*, 129, Article 107863. <https://doi.org/10.1016/j.ecolind.2021.107863>
- Aide, M. T., & Aide, C. (2012). Rare earth elements: Their importance in understanding soil genesis. *International Scholarly Research Notices*, 2012, Article 783876. <https://doi.org/10.5402/2012/783876>
- Alam, A., Bhat, M. S., & Maheen, M. (2020). Using Landsat satellite data for assessing the land use and land cover change in Kashmir valley. *GeoJournal*, 85(6), 1529–1543. <https://doi.org/10.1007/s10708-019-10037-x>
- Alekseev, A., & Chernikhovskii, D. (2021). Assessment of the health status of tree stands based on Sentinel-2B remote sensing materials and the short-wave vegetation index SWVI. *IOP Conference Series: Earth and Environmental Science*, 76(1), Article 012003. <https://doi.org/10.1088/1755-1315/876/1/012003>
- Amit, Y., & Geman, D. (1997). Shape quantization and recognition with randomized trees. *Neural computation*, 9(7), 1545–1588. <https://doi.org/10.1162/neco.1997.9.7.1545>
- Amitrano, D., Martino, G. D., Iodice, A., Mitidieri, F., Papa, M. N., Riccio, D., & Ruello, G. (2014). Sentinel-1 for monitoring reservoirs: A performance analysis. *Remote Sensing*, 6(11), 10676–10693. <https://doi.org/10.3390/rs61110676>
- Aredehey, G., Mezgebu, A., & Girma, A. (2018). Land-use land-cover classification analysis of Giba catchment using hyper

- temporal MODIS NDVI satellite images. *International Journal of Remote Sensing*, 39(3), 810–821.
<https://doi.org/10.1080/01431161.2017.1392639>
- Argamosa, R. J. L., Blanco, A. C., Baloloy, A. B., Candido, C. G., Dumlalag, J. B. L. C., Dimapilis, L. L. C., & Paringit, E. C. (2018). Modelling above ground biomass of mangrove forest using Sentinel-1 imagery. *ISPRS Annals of Photogrammetry, Remote Sensing & Spatial Information Sciences*, 4(3).
<https://doi.org/10.5194/isprs-annals-IV-3-13-2018>
- Assalé, A. A., Barima, Y. S., Sangne, Y. C., Bleu, D. K., & Kpangui, K. B. (2020). Évaluation des services d'approvisionnement fournis par les espaces domaniaux anthropisés: cas de la forêt classée du Haut-Sassandra (Centre-Ouest de la Côte d'Ivoire). *Canadian Journal of Forest Research*, 50(10), 1002–1011.
<https://doi.org/10.1139/cjfr-2019-0443>
- Assi, L. A., & Guinko, S. (1996). Confusion de deux taxons spécifiques ou subsécifiques au sein du genre *Borassus* en Afrique de l'Ouest. In L. J. G. van der Maesen, X. M. van der Burgt, & J. M. van Medenbach de Rooy (Eds.), *The Biodiversity of African Plants* (pp. 773–779). Springer.
https://doi.org/10.1007/978-94-009-0285-5_98
- Atzberger, C. (2013). Advances in remote sensing of agriculture: Context description, existing operational monitoring systems and major information needs. *Remote Sensing*, 5(2), 949–981.
<https://doi.org/10.3390/rs5020949>
- Baccini, A., Goetz, S. J., Walker, W. S., Laporte, N. T., Sun, M., Sulla-Menashe, D., Hackler, J., Beck, P. S. A., Dubayah, R., Friedl, M. A., Samanta, S., & Houghton, R. A. (2012). Estimated carbon dioxide emissions from tropical deforestation improved by carbon-density maps. *Nature Climate Change*, 2(3), 182–185.
<https://doi.org/10.1038/nclimate1354>
- Barima, Y. S. S., Kouakou, A. T. M., Bamba, I., Sangne, Y. C., Godron, M., Andrieu, J., & Bogaert, J. (2016). Cocoa crops are destroying the forest reserves of the classified forest of Haut-Sassandra (Ivory Coast). *Global Ecology and Conservation*, 8, 85–98. <https://doi.org/10.1016/j.gecco.2016.08.009>
- Bourgoin, C., Betbeder, J., Le Roux, R., Gond, V., Oszwald, J., Arvor, D., Baudry, J., Boussard, H., Le Clech, S., & Mazzei, L. (2021). Looking beyond forest cover: An analysis of landscape-scale predictors of forest degradation in the Brazilian Amazon. *Environmental Research Letters*, 16(11), Article 114045.
<https://doi.org/10.1088/1748-9326/ac31eb>
- Breiman, L., Last, M., & Rice, J. (2003). Random forests: Finding quasars. In *Statistical challenges in astronomy* (pp. 243–254). Springer. https://doi.org/10.1007/0-387-21529-8_16
- Breiman, R. F., Cozen, W., Fields, B. S., Mastro, T. D., Carr, S. J., Spika, J. S., & Mascola, L. (1990). Role of air sampling in investigation of an outbreak of Legionnaires' disease associated with exposure to aerosols from an evaporative condenser. *Journal of Infectious Diseases*, 161(6), 1257–1261.
<https://doi.org/10.1093/infdis/161.6.1257>
- Çavur, M., Duzgun, H., Kemeç, S., & Demirkan, D. (2019). Land use and land cover classification of Sentinel 2-A: St Petersburg case study. *The International Archives of Photogrammetry, Remote Sensing and Spatial Information Sciences*, 42, 13–16.
<https://doi.org/10.5194/isprs-archives-XLII-1-W2-13-2019>
- Chaudhary, A., Gustafson, D., & Mathys, A. (2018). Multi-indicator sustainability assessment of global food systems. *Nature Communications*, 9(1), 1–13.
<https://doi.org/10.1038/s41467-018-03308-7>
- Chaudhary, S., & Dhanya, C. (2018). *Dependence of error components in satellite-based precipitation products on topography, LULC and climatic features* [Conference presentation]. AGU Fall Meeting 2018.
- Chemura, A., Mutanga, O., & Odindi, J. (2017). Empirical modeling of leaf chlorophyll content in Coffee (*Coffea Arabica*) plantations with Sentinel-2 MSI data: Effects of spectral settings, spatial resolution, and crop canopy cover. *IEEE Journal of Selected Topics in Applied Earth Observations and Remote Sensing*, 10(12), 5541–5550.
<https://doi.org/10.1109/JSTARS.2017.2750325>
- Chen, Z., & Zhao, S. (2022). Automatic monitoring of surface water dynamics using Sentinel-1 and Sentinel-2 data with Google Earth Engine. *International Journal of Applied Earth Observation and Geoinformation*, 113, Article 103010.
<https://doi.org/10.1016/j.jag.2022.103010>
- Chen, Z., Zhibin, S., Huaqing, Z., Huacong, Z., Huacong, Z., & Hanqing, Q. (2023). Aboveground forest biomass estimation using tent mapping atom search optimized backpropagation neural network with Landsat 8 and Sentinel-1A data. *Remote Sensing*, 15(24), Article 5653. <https://doi.org/10.3390/rs15245653>
- Cheyns, E., Akindes, F., & Aka Adié, F. (2000). La filière palmier à huile en Côte d'Ivoire 3 ans après la privatisation: état des lieux d'un procès de recomposition institutionnelle. *Oléagineux Corps gras Lipides*, 7(2), 166–171.
<https://doi.org/10.1051/oocl.2000.0166>
- Choi, H., & Baraniuk, R. G. (2001). Multiscale image segmentation using wavelet-domain hidden Markov models. *IEEE Transactions on Image Processing*, 10(9), 1309–1321.
<https://doi.org/10.1109/83.941855>
- Chrysafis, I., Mallinis, G., Siachalou, S., & Patias, P. (2017). Assessing the relationships between growing stock volume and Sentinel-2 imagery in a Mediterranean forest ecosystem. *Remote Sensing Letters*, 8(6), 508–517.
<https://doi.org/10.1080/2150704X.2017.1295479>
- Collet, C., & Calloz, R. (2001). *Précis de Télédétection, Volume 3: Traitements Numériques d'Images de Télédétection*. Universités francophones. Presses de l'Université du Québec.
- Congalton, R. G., Gu, J., Yadav, K., Thenkabail, P., & Ozdogan, M. (2014). Global land cover mapping: A review and uncertainty analysis. *Remote Sensing*, 6(12), 12070–12093.
<https://doi.org/10.3390/rs61212070>
- Cutler, D. R., Edwards Jr, T. C., Beard, K. H., Cutler, A., Hess, K. T., Gibson, J., & Lawler, J. J. (2007). Random forests for classification in ecology. *Ecology*, 88(11), 2783–2792.
<https://doi.org/10.1890/07-0539.1>
- Descals, A., Szantoi, Z., Meijaard, E., Sutikno, H., Rindanata, G., & Wich, S. (2019). Oil palm (*Elaeis guineensis*) mapping with details: Smallholder versus industrial plantations and their extent in Riau, Sumatra. *Remote Sensing*, 11(21), Article 2590.
<https://doi.org/10.3390/rs11212590>
- Dhanda, P., Nandy, S., Kushwaha, S., Ghosh, S., Murthy, Y. K., & Dadhwal, V. (2017). Optimizing spaceborne LiDAR and very high resolution optical sensor parameters for biomass estimation at ICESat/GLAS footprint level using regression algorithms. *Progress in Physical Geography*, 41(3), 247–267.
<https://doi.org/10.1177/0309133317693443>
- Dhanya, T., & Yerramalli, C. S. (2018). Lightning strike effect on carbon fiber reinforced composites—effect of copper mesh protection. *Materials Today Communications*, 16, 124–134.
<https://doi.org/10.1016/j.mtcomm.2018.05.009>
- Disse, M., Fenta Mekonnen, D., Duan, Z., & Rientjes, T. (2018). Analysis of the combined and single effects of LULC and climate change on the streamflow of the Upper Blue Nile River Basin (UBNRB): Using statistical trend tests, remote sensing landcover maps and the SWAT model. In *EGU General Assembly Conference Abstracts*, Vienna, Austria.
<https://doi.org/10.5194/hess-2017-685>

- European Space Agency. (2019). *ESA convention and council rules of procedure*. European Space Agency Communications, ESTEK, Noordwijk, The Netherlands.
- Evéillé, F., Schiettecatte, L.-S., & Toudert, A. (2020). *Economic and climate effects of low-carbon agricultural and bioenergy practices in the rice value chain in Gagnoa, Côte d'Ivoire*. Food and Agriculture Organization of the United Nations.
- Falk, R., Wapner, P., & Elver, H. (2016). Climate change, policy knowledge, and the temporal imagination. In P. Wapner & H. Elver (Eds.), *Reimagining climate change*. Routledge. <https://doi.org/10.4324/9781315671468>
- Foga, S., Scaramuzza, P. L., Guo, S., Zhu, Z., Dilley Jr, R. D., Beckmann, T., Schmidt, G. L., Dwyer, J. L., Hughes, M. J. & Laue, B. (2017). Cloud detection algorithm comparison and validation for operational Landsat data products. *Remote Sensing of Environment*, 194, 379–390. <https://doi.org/10.1016/j.rse.2017.03.026>
- Fosgate, C. H., Krim, H., Irving, W. W., Karl, W. C., & Willsky, A. S. (1997). Multiscale segmentation and anomaly enhancement of SAR imagery. *IEEE Transactions on Image Processing*, 6(1), 7–20. <https://doi.org/10.1109/83.552077>
- Gao, Q., Zribi, M., Escorihuela, M. J., & Baghdadi, N. (2017). Synergistic use of Sentinel-1 and Sentinel-2 data for soil moisture mapping at 100 m resolution. *Sensors*, 17(9), Article 1966. <https://doi.org/10.3390/s17091966>
- Garioud, A., Valero, S., Giordano, S., & Mallet, C. (2021). Recurrent-based regression of Sentinel time series for continuous vegetation monitoring. *Remote Sensing of Environment*, 263, Article 112419. <https://doi.org/10.1016/j.rse.2021.112419>
- Ghorbanian, A., Kakooei, M., Amani, M., Mahdavi, S., Mohammadzadeh, A., & Hasanlou, M. (2020). Improved land cover map of Iran using Sentinel imagery within Google Earth Engine and a novel automatic workflow for land cover classification using migrated training samples. *ISPRS Journal of Photogrammetry and Remote Sensing*, 167, 276–288. <https://doi.org/10.1016/j.isprsjprs.2020.07.013>
- Ghosh, A., Fassnacht, F. E., Joshi, P. K., & Koch, B. (2014). A framework for mapping tree species combining hyperspectral and LiDAR data: Role of selected classifiers and sensor across three spatial scales. *International Journal of Applied Earth Observation and Geoinformation*, 26, 49–63. <https://doi.org/10.1016/j.jag.2013.05.017>
- Gorelick, N., Hancher, M., Dixon, M., Ilyushchenko, S., Thau, D., & Moore, R. (2017). Google Earth Engine: Planetary-scale geospatial analysis for everyone. *Remote Sensing of Environment*, 202, 18–27. <https://doi.org/10.1016/j.rse.2017.06.031>
- Grimm, R., Behrens, T., Märker, M., & Elsenbeer, H. (2008). Soil organic carbon concentrations and stocks on Barro Colorado Island – Digital soil mapping using Random Forests analysis. *Geoderma*, 146(1–2), 102–113. <https://doi.org/10.1016/j.geoderma.2008.05.008>
- Grinand, C., Rakotomalala, F., Gond, V., Vaudry, R., Bernoux, M., & Vieilledent, G. (2013). Estimating deforestation in tropical humid and dry forests in Madagascar from 2000 to 2010 using multi-date Landsat satellite images and the random forests classifier. *Remote Sensing of Environment*, 139, 68–80. <https://doi.org/10.1016/j.rse.2013.07.008>
- Gulácsi, A., & Kovács, F. (2020). Sentinel-1-imagery-based high-resolution water cover detection on wetlands, Aided by Google Earth Engine. *Remote Sensing*, 12(10), Article 1614. <https://doi.org/10.3390/rs12101614>
- Haifeng, T., Jianxi, H., Xucao, L., Jian, W., Boyan, Z., Yaochen, Q., & Li, W. (2020). Garlic and winter wheat identification based on active and passive satellite imagery and the Google Earth Engine in Northern China. *Remote Sensing*, 12(21), Article 3539. <https://doi.org/10.3390/rs12213539>
- Han, H.-G., & Lee, M.-J. (2020). A method for classifying land and ocean area by removing Sentinel-1 speckle noise. *Journal of Coastal Research*, 102(SI), 33–38. <https://doi.org/10.2112/SI102-004.1>
- Hermosilla, T., Wulder, M. A., White, J. C., Coops, N. C., & Hobbart, G. W. (2018). Disturbance-informed annual land cover classification maps of Canada's forested ecosystems for a 29-year landsat time series. *Canadian Journal of Remote Sensing*, 44(1), 67–87. <https://doi.org/10.1080/07038992.2018.1437719>
- Huang, H., Chen, Y., Clinton, N., Wang, J., Wang, X., Liu, C., Gong, P., Yang, J., Bai, Y., Zheng, Y., & Zhu, Z. (2017). Mapping major land cover dynamics in Beijing using all Landsat images in Google Earth Engine. *Remote Sensing of Environment*, 202, 166–176. <https://doi.org/10.1016/j.rse.2017.02.021>
- Huang, C., Yang, Q., & Huang, W. (2021). Analysis of the spatial and temporal changes of NDVI and its driving factors in the wei and jing river basins. *International Journal of Environmental Research and Public Health*, 18(22), Article 11863. <https://doi.org/10.3390/ijerph182211863>
- Immitzer, M., Vuolo, F., & Atzberger, C. (2016). First experience with Sentinel-2 data for crop and tree species classifications in central Europe. *Remote Sensing*, 8(3), Article 166. <https://doi.org/10.3390/rs8030166>
- Jiaxin, L., Ling, H., Lei, L., Junfeng, W., Zhaode, X., Dingjian, J., & Xinlin, Z. (2023). Lithology classification in semi-arid area combining multi-source remote sensing images using support vector machine optimized by improved particle swarm algorithm. *International Journal of Applied Earth Observation and Geoinformation*, 119, Article 103318. <https://doi.org/10.1016/j.jag.2023.103318>
- Jović, A., Brkić, K., & Bogunović, N. (2012). Decision tree ensembles in biomedical time-series classification. In A. Pinz, T. Pock, H. Bischof, & F. Leberl (Eds.), *Lecture notes in computer science: Vol. 7476. Pattern Recognition. DAGM/OAGM 2012* (pp. 408–417). Springer. https://doi.org/10.1007/978-3-642-32717-9_41
- Kaplan, G., & Avdan, U. (2017). Object-based water body extraction model using Sentinel-2 satellite imagery. *European Journal of Remote Sensing*, 50(1), 137–143. <https://doi.org/10.1080/22797254.2017.1297540>
- Khan, A., Govil, H., Kumar, G., & Dave, R. (2020). Synergistic use of Sentinel-1 and Sentinel-2 for improved LULC mapping with special reference to bad land class: A case study for Yamuna River floodplain, India. *Spatial Information Research*, 28(6), 669–681. <https://doi.org/10.1007/s41324-020-00325-x>
- Khellouk, R., Barakat, A., El Jazouli, A., Lionboui, H., & Benabdellouahab, T. (2021). Assessment of Water Cloud Model based on SAR and optical satellite data for surface soil moisture retrievals over agricultural area. *Eurasian Journal of Soil Science*, 10(3), 243–250. <https://doi.org/10.18393/ejss.926813>
- Klopper, H. C., Coetzee, S. K., Pretorius, R., & Bester, P. (2012). Practice environment, job satisfaction and burnout of critical care nurses in South Africa. *Journal of Nursing Management*, 20(5), 685–695. <https://doi.org/10.1111/j.1365-2834.2011.01350.x>
- Kolyaie, S., Treier, U. A., Watmough, G. R., Madsen, B., Bøcher, P. K., Psomas, A., Bösch, R., & Normand, S. (2019). Transferability and the effect of colour calibration during multi-image classification of Arctic vegetation change. *Polar Biology*, 42(7), 1227–1239. <https://doi.org/10.1007/s00300-019-02491-7>
- Kopecká, M., Szatmári, D., & Rosina, K. (2017). Analysis of urban green spaces based on Sentinel-2A: Case studies from

- Slovakia. *Land*, 6(2), Article 25.
<https://doi.org/10.3390/land6020025>
- Kouakou, P.-A. (2021). Estimation des effets macroeconomiques de la volatilité des cours internationaux du cacao a l'aide du modele VAR/VECM: selon le cas de la Cote d'Ivoire. In *InterConf* (pp. 29–53). <https://doi.org/10.51582/interconf.7-8.11.2021.003>
- Kouakou, J.-L., Gonedelé Bi, S., Bitty, E. A., Kouakou, C., Yao, A. K., Kassé, K. B., & Ouattara, S. (2020). Ivory Coast without ivory: Massive extinction of African forest elephants in Côte d'Ivoire. *PloS ONE*, 15(10), Article e0232993.
<https://doi.org/10.1371/journal.pone.0232993>
- Kouassi, C. J. A., Khan, D., Achille, L. S., Omifolaji, J. K., & Kebin, Z. (2021a). Forest resources depletion: An ecological model for biodiversity preservation and conservation in Cote D'Ivoire. *Open Journal of Ecology*, 11, 870–890.
<https://doi.org/10.4236/oje.2021.1112052>
- Kouassi, C. J. A., Khan, D., Achille, L. S., Omifolaji, J. K., Espoire, M. M. R. B., Zhang, K. B., Yang, X. H., & Horning, N. (2021b). Conflict-induced deforestation detection in African Côte D'ivoire using landsat images and random forest algorithm: A case in Mount Peko National Park. *Applied Ecology and Environmental Research*, 20(3), 2035–2058.
https://doi.org/10.15666/aeer/2003_20352058
- Kouassi, J.-L., Gyuau, A., Diby, L., Bene, Y., & Kouamé, C. (2021c). Assessing land use and land cover change and farmers' perceptions of deforestation and land degradation in South-West Côte d'Ivoire, West Africa. *Land*, 10(4), Article 429.
<https://doi.org/10.3390/land10040429>
- Laurin, G. V., Puletti, N., Hawthorne, W., Liesenberg, V., Corona, P., Papale, D., Chen, Q., & Valentini, R. (2016). Discrimination of tropical forest types, dominant species, and mapping of functional guilds by hyperspectral and simulated multispectral Sentinel-2 data. *Remote Sensing of Environment*, 176, 163–176.
<https://doi.org/10.1016/j.rse.2016.01.017>
- Lavy, V., & Sand, E. (2019). The effect of social networks on students' academic and non-cognitive behavioural outcomes: Evidence from conditional random assignment of friends in school. *The Economic Journal*, 129(617), 439–480.
<https://doi.org/10.1111/eoj.12582>
- Lefebvre, A., Sannier, C., & Corpetti, T. (2016). Monitoring urban areas with Sentinel-2A data: Application to the update of the Copernicus high resolution layer imperviousness degree. *Remote Sensing*, 8(7), Article 606.
<https://doi.org/10.3390/rs8070606>
- Li, G., Rabe, K. S., Nielsen, J., & Engqvist, M. K. (2019). Machine learning applied to predicting microorganism growth temperatures and enzyme catalytic optima. *ACS Synthetic Biology*, 8(6), 1411–1420. <https://doi.org/10.1021/acssynbio.9b00099>
- Li, W., Dong, R., Fu, H., Wang, J., Yu, L., & Gong, P. (2020). Integrating Google Earth imagery with Landsat data to improve 30-m resolution land cover mapping. *Remote Sensing of Environment*, 237, Article 111563. <https://doi.org/10.1016/j.rse.2019.111563>
- Mansaray, L. R., Yang, L., Kabba, V. T., Kanu, A. S., Huang, J., & Wang, F. (2019). Optimising rice mapping in cloud-prone environments by combining quad-source optical with Sentinel-1A microwave satellite imagery. *GIScience & Remote Sensing*, 56(8), 1333–1354.
<https://doi.org/10.1080/15481603.2019.1646978>
- Mansaray, L. R., Zhang, K., & Kanu, A. S. (2020). Dry biomass estimation of paddy rice with Sentinel-1A satellite data using machine learning regression algorithms. *Computers and Electronics in Agriculture*, 176, Article 105674.
<https://doi.org/10.1016/j.compag.2020.105674>
- Mas, J. (2000). Une revue des méthodes et des techniques de télédétection du changement. *Canadian Journal of Remote Sensing*, 26(4), 349–362.
<https://doi.org/10.1080/07038992.2000.10874785>
- Mengqi, Z., Bao, S., Linsheng, H., Dongyan, Z., Haifeng, X., & Xi-aoying, Y. (2022). Identification of soybean based on Sentinel-1/2 SAR and MSI imagery under a complex planting structure. *Ecological Informatics*, 72, Article 101825.
<https://doi.org/10.1016/j.ecoinf.2022.101825>
- Méger, N., Rigotti, C., Pothier, C., Nguyen, T., Lodge, F., Gueguen, L., Andreoli, R., Doin, M.-R., & Dacru, M. (2019). Ranking evolution maps for Satellite Image Time Series exploration: Application to crustal deformation and environmental monitoring. *Data Mining and Knowledge Discovery*, 33(1), 131–167.
<https://doi.org/10.1007/s10618-018-0591-9>
- Mohammadi, A., & Khodabandehlou, B. (2020). Classification and assessment of land use changes in Zanjan city using object-oriented analysis and Google Earth engine system. *Geography and Environmental Planning*, 31(2), 25–42.
- Mostafa, Y., Ali, M. N. O., Mostafa, F., & Yousef, M. (2022). An approach for building rooftop border extraction from very high-resolution satellite images. *Geocarto International*, 37(15), 4557–4570. <https://doi.org/10.1080/10106049.2021.1892207>
- Murray, N. J., Keith, D. A., Simpson, D., Wilshire, J. H., & Lucas, R. M. (2018). Remap: An online remote sensing application for land cover classification and monitoring. *Methods in Ecology and Evolution*, 9(9), 2019–2027.
<https://doi.org/10.1111/2041-210X.13043>
- N'Guessan, A. E., N'dja, J. K., Yao, O. N., Amani, B. H., Gouli, R. G., Piponiot, C., Zo-Bi, I. C., & Héroult, B. (2019). Drivers of biomass recovery in a secondary forested landscape of West Africa. *Forest Ecology and Management*, 433, 325–331.
<https://doi.org/10.1016/j.foreco.2018.11.021>
- Nonni, F., Malacarne, D., Pappalardo, S. E., Codato, D., Meggio, F., & De Marchi, M. (2018). Sentinel-2 Data analysis and comparison with UAV multispectral images for precision viticulture. *GI Forum*, 6(1), 105–116.
https://doi.org/10.1553/giscience2018_01_s105
- Olofsson, P., Foody, G. M., Herold, M., Stehman, S. V., Woodcock, C. E., & Wulder, M. A. (2014). Good practices for estimating area and assessing accuracy of land change. *Remote sensing of Environment*, 148, 42–57.
<https://doi.org/10.1016/j.rse.2014.02.015>
- Ongolo, S., Kouamé Kouassi, S., Chérif, S., & Giessen, L. (2018). The tragedy of forestland sustainability in postcolonial Africa: Land development, cocoa, and politics in Côte d'Ivoire. *Sustainability*, 10(12), Article 4611. <https://doi.org/10.3390/su10124611>
- Ozesmi, S. L., & Bauer, M. E. (2002). Satellite remote sensing of wetlands. *Wetlands Ecology and Management*, 10(5), 381–402.
<https://doi.org/10.1023/A:1020908432489>
- Pareeth, S., Karimi, P., Shafiei, M., & De Fraiture, C. (2019). Mapping agricultural landuse patterns from time series of Landsat 8 using random forest based hierarchical approach. *Remote Sensing*, 11(5), Article 601. <https://doi.org/10.3390/rs11050601>
- Pattanayak, S. P., & Diwakar, S. K. (2018). Seasonal comparative study of NDVI, NDBI and NDWI of Hyderabad City (Telangana) based on LISS-III image using remote sensing and DIP. *Khuj: An International Peer Reviewed Journal of Geography*, 5(1), 78–86. <https://doi.org/10.5958/2455-6963.2018.00006.1>
- Pazúr, R., Feranec, J., Štych, P., Kopecká, M., & Holman, L. (2017). Changes of urbanised landscape identified and assessed by the Urban Atlas data: Case study of Prague and Bratislava. *Land Use Policy*, 61, 135–146.
<https://doi.org/10.1016/j.landusepol.2016.11.022>

- Perez, D., Lu, Y., Kwan, C., Shen, Y., Koperski, K., & Li, J. (2018). Combining satellite images with feature indices for improved change detection. In *2018 9th IEEE Annual Ubiquitous Computing, Electronics & Mobile Communication Conference (UEMCON)*. <https://doi.org/10.1109/UEMCON.2018.8796538>
- Periyasamy, R., Roy, P. D., Chokkalingam, L., Natarajan, L., Sundar, S., Moorthy, P., & Gowrappan, M. (2021). Transformation analysis on landuse/land cover changes for two decades between 1999 and 2019 CE with reference to aquaculture – Nagapattinam Coast, Southeast India. *Journal of the Indian Society of Remote Sensing*, 49(11), 2831–2845. <https://doi.org/10.1007/s12524-021-01432-4>
- Pesaresi, M., Corbane, C., Julea, A., Florczyk, A. J., Syrris, V., & Soille, P. (2016). Assessment of the added-value of Sentinel-2 for detecting built-up areas. *Remote Sensing*, 8(4), Article 299. <https://doi.org/10.3390/rs8040299>
- Pfeifer, M., Disney, M., Quaife, T., & Marchant, R. (2012). Terrestrial ecosystems from space: A review of earth observation products for macroecology applications. *Global Ecology and Biogeography*, 21(6), 603–624. <https://doi.org/10.1111/j.1466-8238.2011.00712.x>
- Plank, S., Marchese, F., Filizzola, C., Pergola, N., Neri, M., Nolde, M., & Martinis, S. (2019). The July/August 2019 lava flows at the Sciara del Fuoco, Stromboli – Analysis from multi-sensor infrared satellite imagery. *Remote Sensing*, 11(23), Article 2879. <https://doi.org/10.3390/rs11232879>
- Qu, L., Chen, Z., Li, M., Zhi, J., & Wang, H. (2021). Accuracy improvements to pixel-based and object-based lulc classification with auxiliary datasets from Google Earth engine. *Remote Sensing*, 13(3), Article 453. <https://doi.org/10.3390/rs13030453>
- Radoux, J., Chomé, G., Jacques, D. C., Waldner, F., Bellemans, N., Matton, N., Lamarche, C., D'Andrimont, R., & Defourny, P. (2016). Sentinel-2's potential for sub-pixel landscape feature detection. *Remote Sensing*, 8(6), Article 488. <https://doi.org/10.3390/rs8060488>
- Rajbongshi, P., Das, T., & Adhikari, D. (2018). Microenvironmental heterogeneity caused by anthropogenic LULC foster lower plant assemblages in the riparian habitats of lentic systems in tropical floodplains. *Science of the Total Environment*, 639, 1254–1260. <https://doi.org/10.1016/j.scitotenv.2018.05.249>
- Rodriguez-Galiano, V., Chica-Olmo, M., Abarca-Hernandez, F., Atkinson, P. M., & Jeganathan, C. (2012a). Random forest classification of mediterranean land cover using multi-seasonal imagery and multi-seasonal texture. *Remote Sensing of Environment*, 121, 93–107. <https://doi.org/10.1016/j.rse.2011.12.003>
- Rodriguez-Galiano, V., Ghimire, B., Pardo-Iguzquiza, E., Chica-Olmo, M., & Congalton, R. G. (2012b). Incorporating the down-scaled Landsat TM thermal band in land-cover classification using random forest. *Photogrammetric Engineering & Remote Sensing*, 78(2), 129–137. <https://doi.org/10.14358/PERS.78.2.129>
- Rodriguez-Galiano, V. F., Ghimire, B., Rogan, J., Chica-Olmo, M., & Rigol-Sanchez, J. P. (2012c). An assessment of the effectiveness of a random forest classifier for land-cover classification. *ISPRS Journal of Photogrammetry and Remote Sensing*, 67, 93–104. <https://doi.org/10.1016/j.isprsjprs.2011.11.002>
- Rosan, T. M., Goldewijk, K. K., Ganzenmüller, R., O'Sullivan, M., Pongratz, J., Mercado, L. M., Aragao, L. O. C., Heinrich, V., Von Randow, C., & Wiltshire, A. (2021). A multi-data assessment of land use and land cover emissions from Brazil during 2000–2019. *Environmental Research Letters*, 16(7), Article 074004. <https://doi.org/10.1088/1748-9326/ac08c3>
- Ruf, F., Salvan, M., Kouamé, J., & Duplan, T. (2020). Qui sont les planteurs de cacao de Côte d'Ivoire? *Papiers de recherche* (pp. 1–11). Éditions AFD. <https://doi.org/10.3917/afd.thier.2020.01.0001>
- Ruf, F., & Varlet, F. (2017). *The myth of zero deforestation cocoa in Côte d'Ivoire*.
- Sallustio, L., Quatrini, V., Geneletti, D., Corona, P., & Marchetti, M. (2015). Assessing land take by urban development and its impact on carbon storage: Findings from two case studies in Italy. *Environmental Impact Assessment Review*, 54, 80–90. <https://doi.org/10.1016/j.eiar.2015.05.006>
- Sánchez-García, E., Palomar-Vázquez, J., Pardo-Pascual, J. E., Almonacid-Caballer, J., Cabezas-Rabadán, C., & Gómez-Pujol, L. (2020). An efficient protocol for accurate and massive shoreline definition from mid-resolution satellite imagery. *Coastal Engineering*, 160, Article 103732. <https://doi.org/10.1016/j.coastaleng.2020.103732>
- Sanial, E., Ruf, F., Louppe, D., Miettinen, M., & Hérault, B. (2023). Local farmers shape ecosystem service provisioning in West African cocoa agroforests. *Agroforestry Systems*, 97, 401–414. <https://doi.org/10.1007/s10457-021-00723-6>
- Schneider, A. (2012). Monitoring land cover change in urban and peri-urban areas using dense time stacks of Landsat satellite data and a data mining approach. *Remote Sensing of Environment*, 124, 689–704. <https://doi.org/10.1016/j.rse.2012.06.006>
- Schucknecht, A., Meroni, M., & Rembold, F. (2016). *Monitoring project impact on biomass increase in the context of the Great Green Wall for the Sahara and Sahel Initiative in Senegal*. European Commission Joint Research Centre, Ispra, Italy.
- Schultz, M., Clevers, J. G., Carter, S., Verbesselt, J., Avitabile, V., Quang, H. V., & Herold, M. (2016). Performance of vegetation indices from Landsat time series in deforestation monitoring. *International Journal of Applied Earth Observation and Geoinformation*, 52, 318–327. <https://doi.org/10.1016/j.jag.2016.06.020>
- Selvakumaran, S., Plank, S., Geiß, C., Rossi, C., & Middleton, C. (2018). Remote monitoring to predict bridge scour failure using Interferometric Synthetic Aperture Radar (InSAR) stacking techniques. *International Journal of Applied Earth Observation and Geoinformation*, 73, 463–470. <https://doi.org/10.1016/j.jag.2018.07.004>
- Shalaby, A., & Tateishi, R. (2007). Remote sensing and GIS for mapping and monitoring land cover and land-use changes in the Northwestern coastal zone of Egypt. *Applied Geography*, 27(1), 28–41. <https://doi.org/10.1016/j.apgeog.2006.09.004>
- Sharma, N., Cao, S., Msallem, B., Kunz, C., Brantner, P., Honigmann, P., & Thieringer, F. M. (2020). Effects of steam sterilization on 3D printed biocompatible resin materials for surgical guides – An accuracy assessment study. *Journal of Clinical Medicine*, 9(5), Article 1506. <https://doi.org/10.3390/jcm9051506>
- Slama, S. B., Choubani, F., Benavente-Peces, C., & Abdelkarim, A. (2021). *Innovative and Intelligent Technology-Based Services For Smart Environments-Smart Sensing and Artificial Intelligence. Proceedings of the 2nd International Conference on Smart Innovation, Ergonomics and Applied Human Factors (SEAHF'20), held online, 14–15 November 2020*. CRC Press. <https://doi.org/10.1201/9781003181545>
- Sonwa, D. J., Dieye, A., El Mzouri, E.-H., Majule, A., Mugabe, F. T., Omolo, N., Wouapi, H., Obando, J., & Brooks, N. (2017). Drivers of climate risk in African agriculture. *Climate and Development*, 9(5), 383–398. <https://doi.org/10.1080/17565529.2016.1167659>

- Tano, A. M. (2012). *Crise cacaoyère et stratégies des producteurs de la sous-préfecture de Méadji au Sud-Ouest ivoirien*. Université Toulouse le Mirail, Toulouse 2, Français.
- Tatsumi, K., Yamashiki, Y., Torres, M. A. C., & Taïpe, C. L. R. (2015). Crop classification of upland fields using Random forest of time-series Landsat 7 ETM+ data. *Computers and Electronics in Agriculture*, 115, 171–179. <https://doi.org/10.1016/j.compag.2015.05.001>
- Tesfamichael, S. G., Newete, S. W., Adam, E., & Dubula, B. (2018). Field spectroradiometer and simulated multispectral bands for discriminating invasive species from morphologically similar cohabitant plants. *GIScience & Remote Sensing*, 55(3), 417–436. <https://doi.org/10.1080/15481603.2017.1396658>
- Tian, H., Banger, K., Bo, T., & Dadhwal, V. K. (2014). History of land use in India during 1880–2010: Large-scale land transformations reconstructed from satellite data and historical archives. *Global and Planetary Change*, 121, 78–88. <https://doi.org/10.1016/j.gloplacha.2014.07.005>
- Veci, L., Prats-Iraola, P., Scheiber, R., Collard, F., Fomferra, N., & Engdahl, M. (2014). The sentinel-1 toolbox. In *Proceedings of the IEEE International Geoscience and Remote Sensing Symposium (IGARSS)*. IEEE.
- Vizzari, M., & Sigura, M. (2015). Landscape sequences along the urban–rural–natural gradient: A novel geospatial approach for identification and analysis. *Landscape and Urban Planning*, 140, 42–55. <https://doi.org/10.1016/j.landurbplan.2015.04.001>
- Wang, Z., Han, Q., & de Vries, B. (2019). Land use/land cover and accessibility: Implications of the correlations for land use and transport planning. *Applied Spatial Analysis and Policy*, 12(4), 923–940. <https://doi.org/10.1007/s12061-018-9278-2>
- Wessel, M., & Quist-Wessel, P. F. (2015). Cocoa production in West Africa, a review and analysis of recent developments. *NJAS-Wageningen Journal of Life Sciences*, 74, 1–7. <https://doi.org/10.1016/j.njas.2015.09.001>
- Xiong, J., Thenkabail, P. S., Gumma, M. K., Teluguntla, P., Poehnel, J., Congalton, R. G., Yadav, K., & Thau, D. (2017). Automated cropland mapping of continental Africa using Google Earth Engine cloud computing. *ISPRS Journal of Photogrammetry and Remote Sensing*, 126, 225–244. <https://doi.org/10.1016/j.isprsjprs.2017.01.019>